ROMANIAN JOURNAL OF INFORMATION SCIENCE AND TECHNOLOGY
Volume **17**, Number 4, 2014, 389–404

Beam Shaping for Phase Singularities

Rebeca TUDOR[1,2], Mihai KUSKO[1], Cristian KUSKO[1], Florea CRACIUNOIU[1], Andrei AVRAM[1], Dan VASILACHE[1], Adrian DINESCU[1]

[1] National Institute for Research and Development in Microtechnologies, Bucharest, Romania
[2] University of Bucharest, Faculty of Physics, Bucharest, Romania

E-mail: {rebeca.tudor, mihai.kusko, cristian.kusko, florea.craciunoiu, andrei.avram, dan.vasilache, adrian.dinescu}@imt.ro

Abstract. In this paper we are molding the phase profile of a Gaussian beam in order to achieve a phase singularity called optical vortex. For this purpose, we apply the beam shaping technique for a 635 nm wavelength radiation using a diffractive optical element with high diffractive efficiency. We use reflective spiral phase plates and fork-like computer generated holograms, fabricated with photolithographic processes and electron beam lithography, respectively. Uniform ring intensity is achieved in the optical vortex configurations and also zero intensity where the phase is undefined. Phase singularities interferences are done using a Michelson interferometer. Beam shaping simulations results based on the Kirchhoff integral are in concordance with experimental results.

Key words: Beam shaping; Optical vortex; Orbital angular momentum; Spiral phase plate; Computer generated hologram; Michelson interferometer.

1. Introduction

The beam shaping technique consists in the redistributing of the intensity and phase of a laser beam in order to achieve a desired form [1]. The beam form is given by the intensity distribution profile, whereas the phase establishes the way of beam propagation. Converting a Gaussian beam into a beam with uniform amplitude and phase is a typical beam shaping example [2– 4]. In this paper we study the optical vortex beam shaping which involves a Gaussian beam diffracted by a spiral phase plate or by a fork-like computer generated hologram. The result consists in uniform

ring intensity with a dark spot in the middle which corresponds to zero intensity due to the phase singularity.

The orbital angular momentum, the parameter of a phase singularity, is one of the most fundamental physical quantities along with energy and momentum in the classical and quantum electromagnetism [5]. The equation of the orbital angular momentum, in the vacuum, can be written like this:

$$\vec{M} = \varepsilon_0 \vec{r} \times \left(\vec{E} \times \vec{B} \right), \tag{1}$$

where $\vec{E}$ and $\vec{B}$ represent electrical and magnetic fields, and ε_0 is the vacuum electric permittivity. The total orbital angular momentum is written:

$$J = \varepsilon_0 \int \vec{r} \times (\vec{E} \times \vec{B}) \mathrm{d}\vec{r}. \tag{2}$$

In the atomic physics, the canonical form of the photon total orbital angular momentum, J_{photon}, has a spin angular momentum – SAM, S_{photon}, and an orbital angular momentum – OAM, L_{photon} [6] as follows:

$$J_{photon} = S_{photon} + L_{photon} \tag{3}$$

The SAM is associated with the circular or elliptical polarization, and has $\pm\hbar$ value, where $\hbar$ is Planck's constant h divided by 2π. The positive SAM value indicates the left polarization whereas the negative SAM value the right polarization [7,8]. The OAM defines the spatial distribution of the electric field of $m\hbar$ per photon, where m, the topological charge, can take any integer value [6, 9]. The OAM carrying beams have a phase singularity represented through a donut shape or a ring shape. Examples of these kinds of beams are Laguerre-Gauss beams, Bessel beams, Mathieu beams, and Ince-Gaussian beams. The optical vortex beams have many technological applications in areas like optical tweezers [10–12], atom manipulation [13, 14], microscopy [15], free-space optical communications [16–18], quantum communications [19], laser beam shaping [20], etc. The methods to generate optical vortices involve the use of spiral phase plates [21] and computer generated holograms [22].

We used both methods to generate optical vortex configurations. Firstly, we achieved optical vortices with a well defined topological charge $m = 2$, $m = 4$, respectively, using two spiral phase plates (SPPs) which were fabricated with standard photolithographical processes. The structural and functional characterisation of the SPPs proved their optical quality. The superposition of an optical vortex with a Gaussian beam in a Michelson interferometer using the fabricated SPPs was useful to determine the topological charge value of the phase singularities. Secondly, we generate optical vortices using a fork-like computer generated hologram (CGH) fabricated in a EBL process.

2. Optical vortex beam shaping simulations

We study the optical vortex beam shaping numerically, by diffracting a Gaussian beam on a spiral phase plate or on a fork-like computer generated hologram using a MATLAB code. We calculate optical vortex configurations using the Kirchhoff's diffraction integral. The electromagnetic field amplitude value at a distance z from the SPP, or from fork-like CGH, is proportional with the electromagnetic field amplitude in the SPP or CGH plane. The equation (4) shows the relation between the electromagnetic field amplitude in a specific point (x, y, z) in the image plane and the amplitude distribution $G(x', y', 0)$ in the object plane (SPP, or CGH plane). $G(x', y', 0)$ is the electromagnetic field amplitude distribution for a SPP: $\exp(\arctan(y'/x'))$, or in the case of CGH $[\exp(ikx') + \exp(im\theta)]^2$.

$$G(x, y, z) = A(x, y, z)\, e^{ikz} \iint_A G(x', y', 0)\, e^{-\frac{x'^2 + y'^2}{w^2}}\, e^{-jk\frac{x'x + y'y}{2z}} dx'dy' . \qquad (4)$$

2.1. Optical vortices generated with SPP simulations

We calculated numerically the spiral phase plate configurations in order to generate optical vortices with topological charges $m = 2$, $m = 4$ respectively, as it can be observed in Fig. 1. The SPPs were considered as a discrete variation of height in 8 levels and $m \times 2\pi$ phase shifts of the optical path. The number of phase shifts represents the topological charge of an optical vortex.

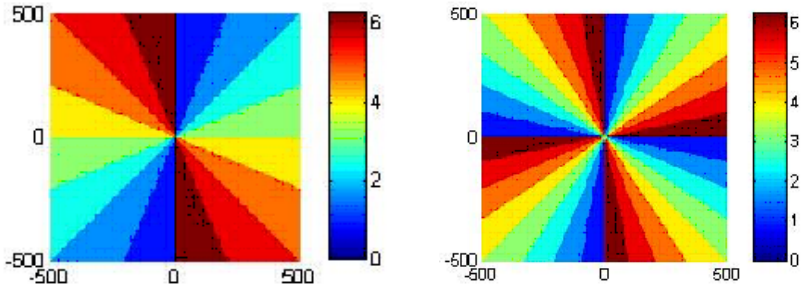

a) b)

Fig. 1. Simulated spiral phase plates which generate optical vortices with topological charge: (a) $m = 2$; (b) $m = 4$.

In Fig. 1a 2π phase difference appears between maximum (red color) and minimum (blue color). In Fig. 1a the SPP has two switches from maximum height to minimum height which means that a Gaussian beam diffracted by this SPP will generate an optical vortex with $m = 2$ topological charge. Likewise the Fig. 1b the four switches of the SPP from maximum height to minimum height means that a Gaussian beam diffracted by this SPP will generate an optical vortex with $m = 4$ topological charge.

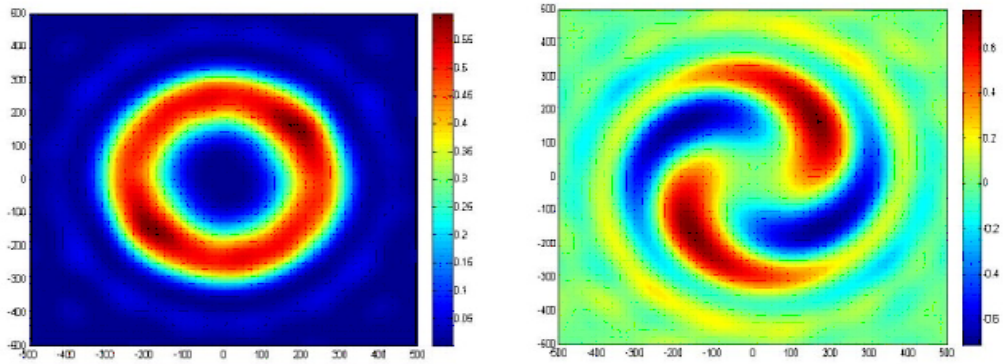

a) b)

Fig. 2. Optical vortex with topological charge $m = 2$: (a) intensity; (b) real part of the field.

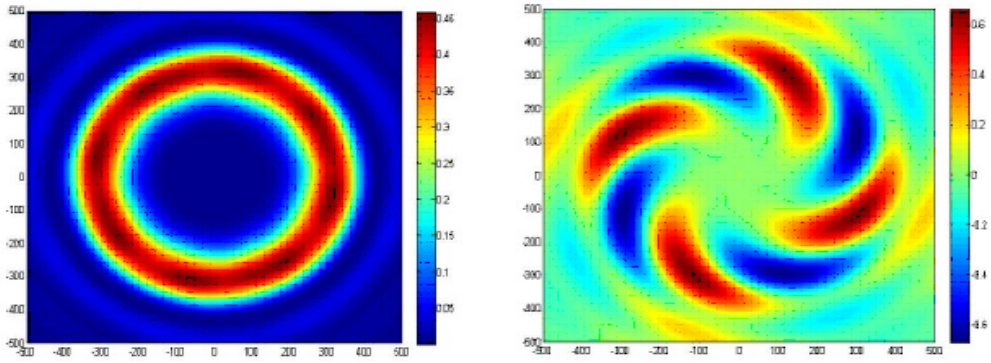

a) b)

Fig. 2′. Optical vortex with topological charge m=4: (a) intensity; (b) real part of the field.

Figures 2 and 2′ contain far field images. The distance z from object (SPP) plane to the image plane is considered much bigger than the size of the SPP. Figures 2a and 2′a represent the intensity of a Gaussian beam diffracted by a spiral phase plate which generates an optical vortex with $m = 2$, $m = 4$ respectively, topological charge. The ring diameter for $m = 4$ is larger than that of the ring with $m = 2$, which proves that the optical vortex diameter increases with the topological charge. The real part of the electromagnetic field of the vortex configuration contains the number of minimum and maximum values of the field. The switch between a maximum and a minimum value indicates a 2π phase shift. In Fig. 2b there are $2 \times 2\pi$ phase shifts, which means that the optical vortex has a $m = 2$ topological charge. In Fig. 2′b there are $4 \times 2\pi$ phase shifts, which means that the optical vortex has a $m = 4$ topological charge.

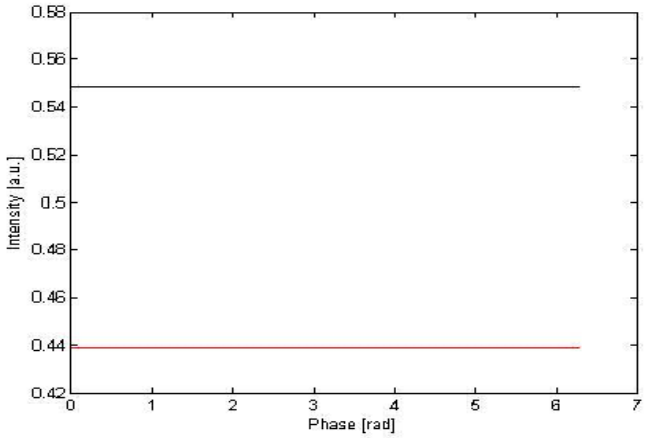

Fig. 3. Radial profile for the maximum intensity for $m = 2$ – black line, $m = 4$ – red line.

The intensity is constant in the annular configuration of an optical vortex for a radial profile. In Fig. 3 it can be observed the maximum intensity with a 0.5485 [a.u.] constant value for $m = 2$ topological charge represented by the black line and a 0.4391 [a.u.] constant value for $m = 4$ topological charge represented by the red line. The intensity of $m = 4$ is lower than for $m = 2$ due to its larger diameter, proportional with the topological charge, which proves that the power of the beam is conserved.

2.2. Optical vortices generated with fork-like computer generated holograms (CGHs)

The fork-like computer generated hologram represents the superposition of a plane wave $f_1 = \exp(ikx)$, and a helical phase wave $f_2 = \exp(im\theta)$. In the plane wave formula, k represents the spatial frequency which determines the spatial separation of the spots in the diffraction pattern. In the case of the helical beam formula, m represents the number of twists that the beam does in a wavelength of propagation, which is also called topological charge. θ indicates the azimuthal position and takes values in the [0, 2π] range. The fork-like computer generated holograms can be observed in Fig. 4, being calculated numerically using the equation (5):

$$H = |f_1 + f_2|^2 = \left|e^{ikx} + e^{im\theta}\right|^2 \tag{5}$$

The difference between the number of fringes of emerging on the upper side of the CGH from the central singularity and the ones emerging on the lower side of the CGH establishes the topological charge of an optical vortex. In Fig. 4a, the fork-like CGH has three black fringes, so a Gaussian beam diffracted by this diffractive optical element will generate optical vortices with topological charges ± 2. In Fig. 4b, the fork-like computer hologram has five bright fringes, so the diffraction pattern will have optical vortices with topological charges $m = \pm 4$.

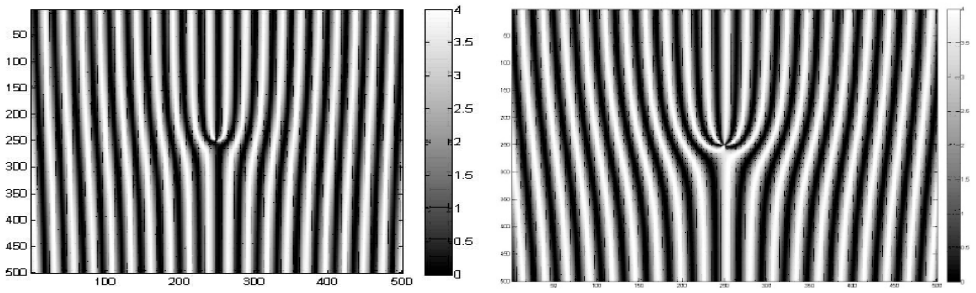

a) b)

Fig. 4. Fork-like CGHs which generate optical vortices with topological charge: (a) $m = 2$; (b) $m = 4$.

In Fig. 5, it can be observed a diffraction pattern as a result of a Gaussian beam and fork-like CGH interaction, containing optical vortices with topological charge $m = \pm 4$. In Fig. 5a is represented the intensity profile having an optical vortex with $m = -4$ topological charge in the left side, a Gaussian beam in the centre, and an optical vortex with $m = 4$ topological charge in the right side. The real part of these vortex configurations is represented in Fig. 5b. Both optical vortices have four red maximum peaks and 4 blue minimum peaks. The difference between the $m = -4$ optical vortex and the $m = 4$ optical vortex is the twist direction.

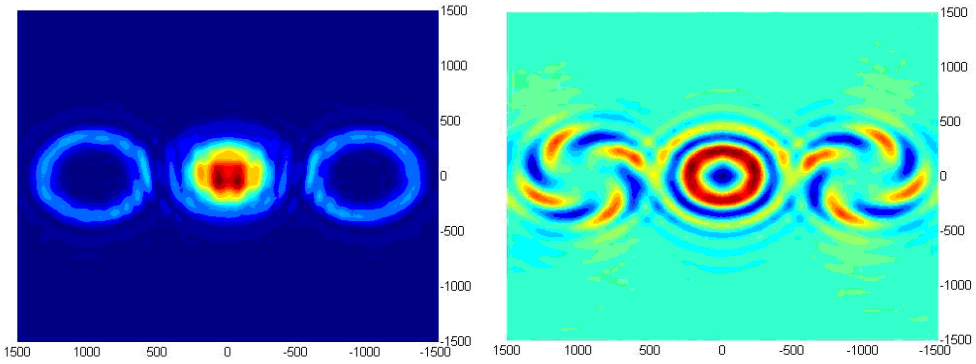

a) b)

Fig. 5. Diffraction pattern of a fork-like CGH with 4 fringes: (a) Intensity; (b) Real part.

The Matlab simulations based on Kirchhoff's diffraction integral permit the determination of the geometrical parameters necessary for the fabrication process of the diffractive optical elements presented above (SPP, fork-like CGH). The fabrication techniques such as photolithography and RIE for the SPP fabrication and EBL for the fork-like fabrication are reliable. The high quality of the devices is proved by structural and functional characterisations. The fabrication processes of these elements are described below.

3. Fabrication and characterisation of the SPPs

3.1. Fabrication process of the SPPs

A spiral phase plate has a spiral configuration due to a azimuthal variation of heigth, h, which depends on m, the desired topological charge, λ, the incident wavelength on the SPP, θ, the azimuthal position, n, the refractive index:

$$h = m\lambda\theta/[2\pi(n-1)] \tag{6}$$

We fabricated two SPPs which permit the generation of the phase singularities with $m = 2$, $m = 4$ respectively, topological charge. For this purpose we designed three photolithographical masks in order to achieve 2^3 levels. The number of levels is restricted due to the fabrication limitations. Even though the optical path variation is not continue, the functional characterisation of the SPPs reveals that this number of levels is sufficient for the generation of optical vortices with a well defined topological charge. The photolithographical masks were designed in the CleWin software in order to fabricate SPPs with 1 cm $\times$ 1 cm dimensions with 8 levels geometry. The fabrication involved three successive technological processes (photolithography and reactive ion etching – RIE) for each photolithographical mask presented in Fig. 6.

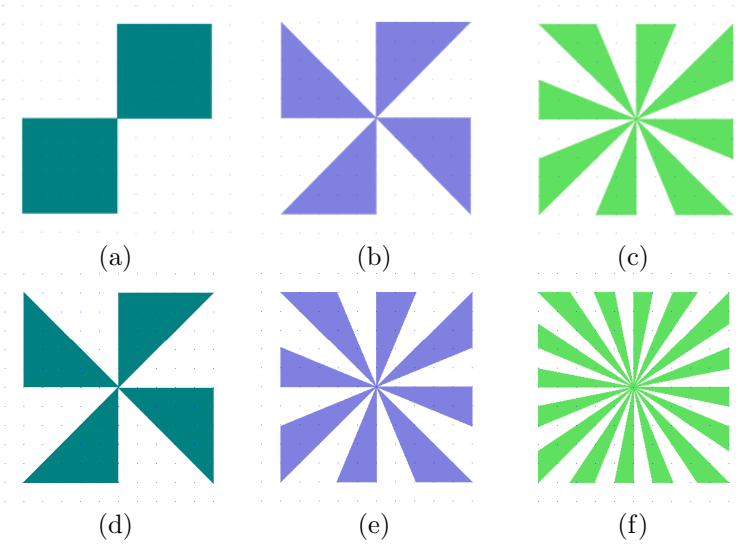

Fig. 6. Photolithographical masks used for SPPs fabrication: (a), (b),(c) first, second, third mask, for a $m = 2$ topological charge optical vortex generation; (d), (e), (f), first, second, third mask, for a $m = 4$ topological charge optical vortex generation [23].

For the SPPs fabrication we used a 3 inches silicon wafer. On this substrate we achieved a 1.2 µm thickness layer of silicon dioxide, after a thermal oxidation at 1100°C temperature. The spiral geometry of the SPPs was facilitated by a calibrated reactive ion etching process. The RIE technique permits a precise etching rate. The

process parameters were: SF_6:O_2 (9:1), p=20 Pa, P=200 W. They were perfect suitable for low etching depths like tens of nanometers and were set in a way that the difference between two consecutive levels of the SPP should be 40 nm and the difference between the maximum level and the minimum level should be 280 nm. In the end a metallization was done in order to achieve a good reflectivity depositing a 10 nm thickness layer of Cr and a 50 nm thickness layer of Au.

The technological process presented above is perfect reproducible. Similar results were achieved when the process was repeated after a period of time.

3.2. Structural characterization

We performed a morphological characterization for the SPPs using the white light interferometry (WLI). This method gives quantitative information about the SPP geometry in a sense that a precise value for each etched depth can be determined. Figures 7 and 7′ illustrate the SPPs WLI morphological characterization. in a three dimensional configuration.

In Fig. 7 the SPP has two switches from the maximum height (pink-red color) to the minimum height (blue color). This means that a Gaussian beam diffracted by this SPP will generate an optical vortex with $m = 2$ topological charge.

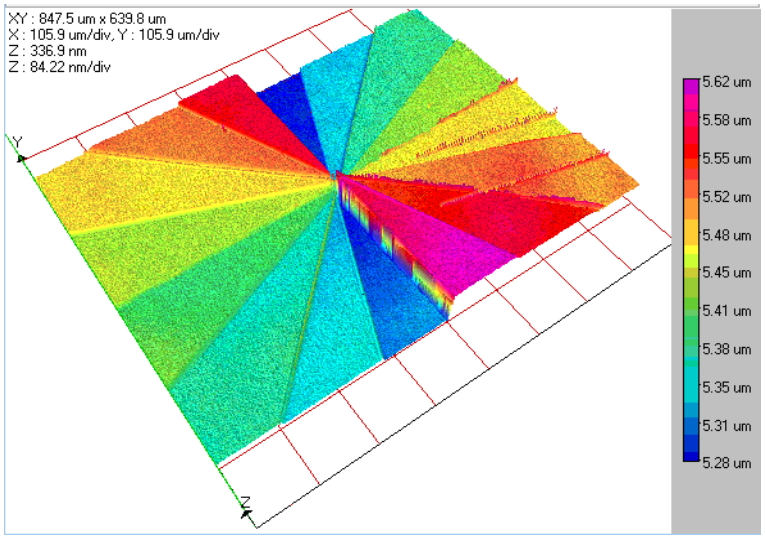

Fig. 7. WLI image for SPP which generates optical vortices with m=2: 3D profile.

Table 1. Cross section: level differences (from left to right) for a) $m = 2$, optical vortex generation

(nm)→	1	2	3	4	5	6	7
Δz (S2)	42.4	31.5	37.8	283.6	32.3	29.3	33.5

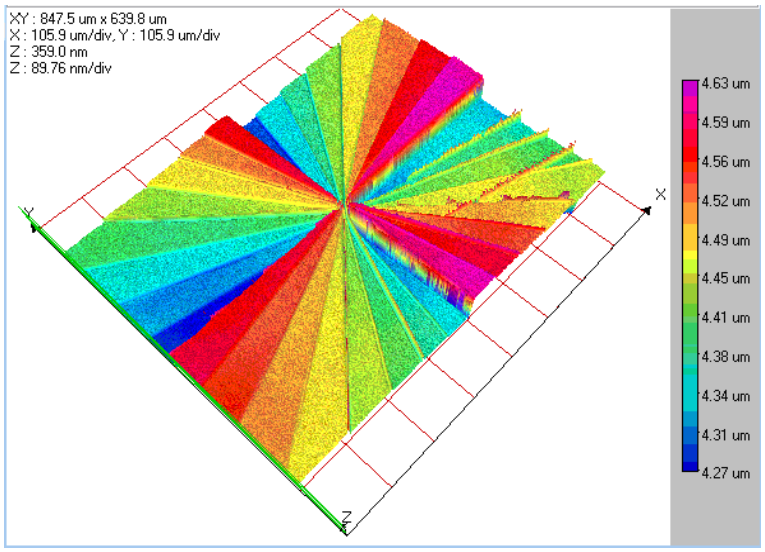

Fig. 7′. WLI image for SPP which generates optical vortices with $m = 4$: 3D profile.

In Fig. 7′ the SPP has four switches from the maximum height (pink-red color) to the minimum height (blue color). This means that a Gaussian beam diffracted by this SPP will generate an optical vortex with $m = 4$ topological charge.

Table 2. Cross section: level differences (from left to right) for a) $m = 4$, optical vortex generation

(nm)→	1	2	3	4	5	6	7	8	9	10	11	12	13
Δz (S4)	38.3	41.6	49.5	46.8	42.7	37.4	281.3	45.2	42.6	46.6	40.0	51.6	37.8

A cross section of the SPP shows the etching depths values for the $m = 2$ case can be observed in Table 1 and for the $m = 4$ case in the Table 2. It is revealed that the difference between the maximum and the minimum level is 280 nm , and the difference between two consecutive levels is 30–50 nm.

These results prove that the fabricated SPPs satisfy geometrical conditions established after the simulation results regarding the optical vortex generation.

3.3. Functional characterization

3.3.1. Optical vortex generation

An optical set-up was done in order to functional characterize the SPPs, which can be observed in Diagram 1. A 635 nm wavelength laser beam is collimated with a collimator. After that the Gaussian beam passes through an aperture, and a 2 mm spot is achieved; then is diffracted by a reflective SPP in order to generate an optical vortex with $m = 2$, $m = 4$ respectively topological charge. The optical vortex captures as it can be observed in Fig. 7, are far field images – approximately 15 m away from the SPPs plane.

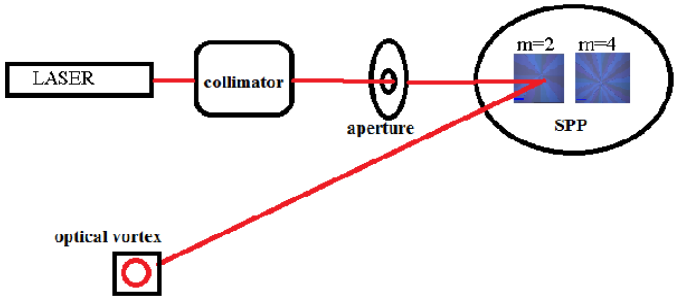

Diagram 1. Experimental set-up for an optical vortex generation.

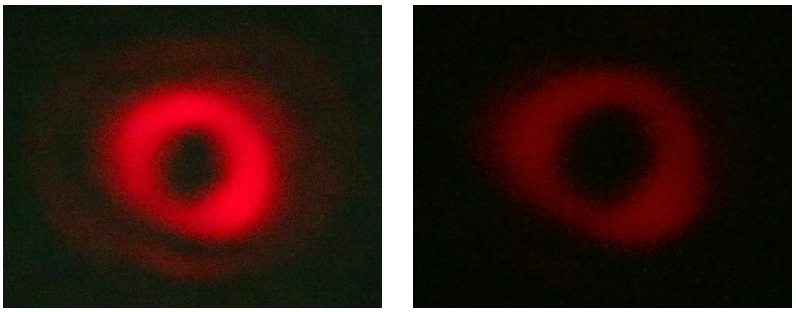

(a) (b)

Fig. 8. Far field images of the optical vortices with the topological charge (a) $m = 2$; (b) $m = 4$.

In Fig. 8 are illustrated the far field images of optical vortices which represent a laser beam diffracted by the SPPs. It can be observed their annular configuration and the fact that the diameter of the optical vortex with the $m = 2$ topological charge is visible smaller than the diameter of the optical vortex with $m = 4$ topological charge. This is in perfect concordance with the optical vortices theory.

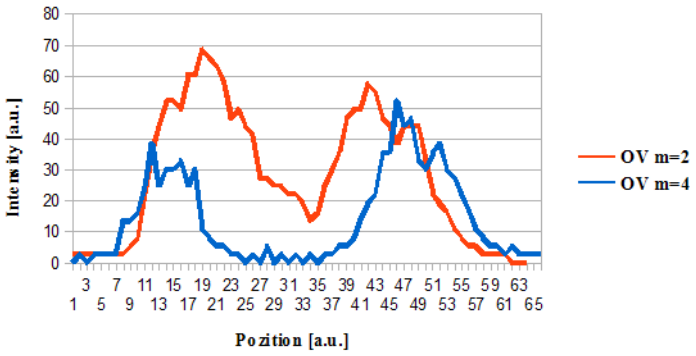

Fig. 9. Far field cross section of the optical vortices with the topological charge: $m = 2$, $m = 4$ respectively.

In the Fig. 9, a far field cross section of the optical vortices configuration was done. It can be observed that the intensity of $m = 2$ is bigger than for $m = 4$ and its smaller diameter, inverse proportional with the topological charge. This is a proof that the power of the beam is conserved.

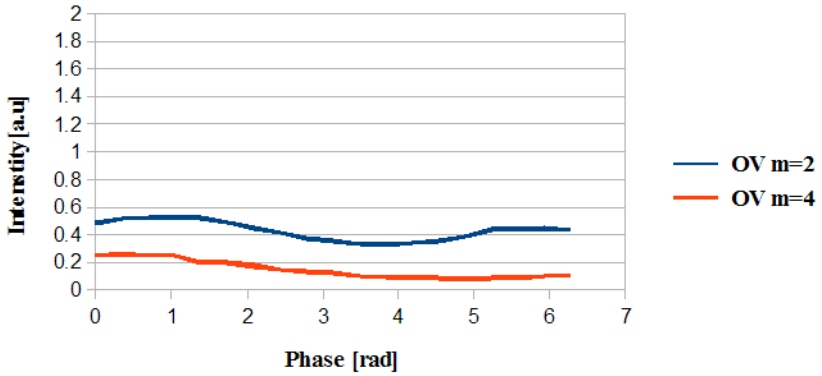

Fig. 10. Far field radial cross section of the optical vortices with the topological charge: $m = 2$, $m = 4$ respectively.

The optical vortex beam shaping involves a uniform intensity in the annular configuration of an optical vortex for a specific radius. In Fig. 10, it can be observed the intensity of an optical vortex with $m = 2$ topological charge represented by the blue line, respective for an optical vortex with $m = 4$ topological charge represented by the red line. The average value of the intensity in arbitrary units for $m = 2$ case is 0.4268 [a.u.], whereas for $m = 4$ case is 0.1463 [a.u.]. The intensity of $m = 4$ is lower than for $m = 2$ as a consequence of its larger diameter, proportional with the topological charge. This is also evidence that the power of the beam is conserved.

3.3.2. Detection of the topological charge

Interference patterns of optical vortices with Gaussian beams were obtained using a Michelson interferometer in order to determine their topological charges.

Essentially, the Michelson interferometer experimental set-up in which interference between a Gaussian beam and an optical vortex takes place consists of a beam splitter, a mirror and a reflective spiral phase plate. A 635 wavelength Gaussian beam is divided in two identical Gaussian beams using a 50:50 beam splitter. The first Gaussian beam is diffracted by a SPP with order $m = 4$ and generates an optical vortex. The second Gaussian beam is diffracted by a mirror and remains a Gaussian beam which interferes with the (phase singularity) optical vortex. The interference image is illustrated in Fig. 12 and represents the detection of the topological charge for an optical vortex.

A fork-like configuration is generated by the interference between a Gaussian beam and an optical vortex beam. The topological charge of the optical vortex corresponds to the number of fringes emerging from the central singularity minus 1. In Fig. 11

is illustrated the interference figure between a Gaussian beam and an optical vortex beam with the topological charge optical $m = 4$, in near field 10 cm away from the SPPs plane.

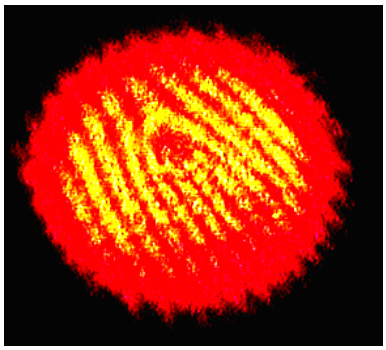

Fig. 11. The interference figure between a Gaussian beam and an optical vortex beam with the topological charge optical $m = 4$, in near field – 10 cm.

4. EBL fork-like computer generated hologram fabrication

4.1. Fabrication

We fabricated a fork-like computer generated hologram using a reliable nanofabrication technique such as the electron beam lithography [24]. On a silicon wafer, it was deposited an electronresist layer of 320 nm thickness in order to achieve two levels with the optical path difference between the upper level and the lower level of 640 nm. This corresponds to the incident beam wavelength. The phase difference between these two levels is 2π and the hologram works in reflection mode.

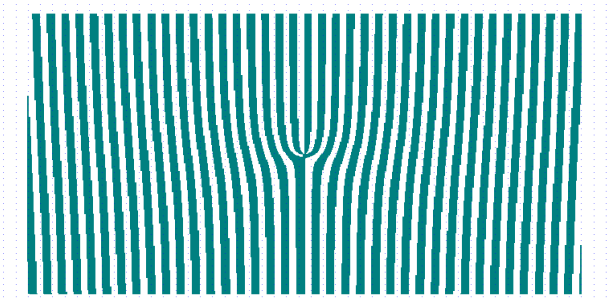

Fig. 12. The EBL mask for a fork-like computer hologram which generates optical vortices with $m = 4$ topological charge.

The configuration of this hologram has been calculated according to the equation (8), being the interference between a plane wave and a helical wave with a specific orbital angular momentum. For the dark fringes of the hologram $\exp(ik_x x) +$

$\exp(im\theta)| < 1$, whereas for the bright fringes of the hologram $|\exp(ik_x x)+\exp(im\theta)| > 1$. k_x represents the spatial frequency, m is the topological charge, and $\theta = \arctan(y/x)$. In Fig. 12 is presented the fork-like computer generated hologram used as EBL for $m = 4$.

The electron beam lithography was done with a 250 $\mu C/cm^2$ exposure dose, using a 20 kV acceleration voltage, a 5 kV extraction voltage and a 20 pA electron beam current. In the end a metallization was done with a 80 nm thickness aluminum layer in order to have a good reflectivity.

4.2. Characterization

4.2.1. Structural characterization

The fabricated hologram was characterized structurally and functionally. The structural characterization is represented in Fig. 13 and Fig. 14. The optical image of the fork-like computer hologram is illustrated in Fig. 13 and the scanning electron microscopy (SEM) image is illustrated in Fig. 14. It can be observed a perfect concordance between the EBL mask and the fabricated hologram.

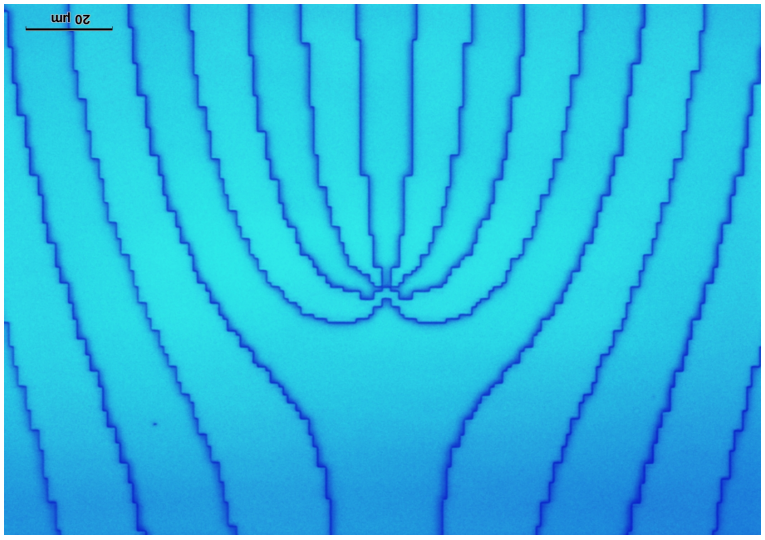

Fig. 13. The optical image of the fork-like computer hologram which generates optical vortices with $m = 4$ topological charge.

4.2.2. Functional characterization

The functional characterization of the reflective hologram was done using a 632 nm wavelength radiation. A Gaussian beam was diffracted on the hologram and as a result an optical vortex with topological charge $m = -4$ in the left, for the $n = -1$ order of diffraction, Gaussian beam with $m = 0$, for $n = 0$, and an optical vortex

with $m = 4$ for the order of diffraction $n = 1$ were achieved. The far field diffraction image is illustrated in Fig. 15.

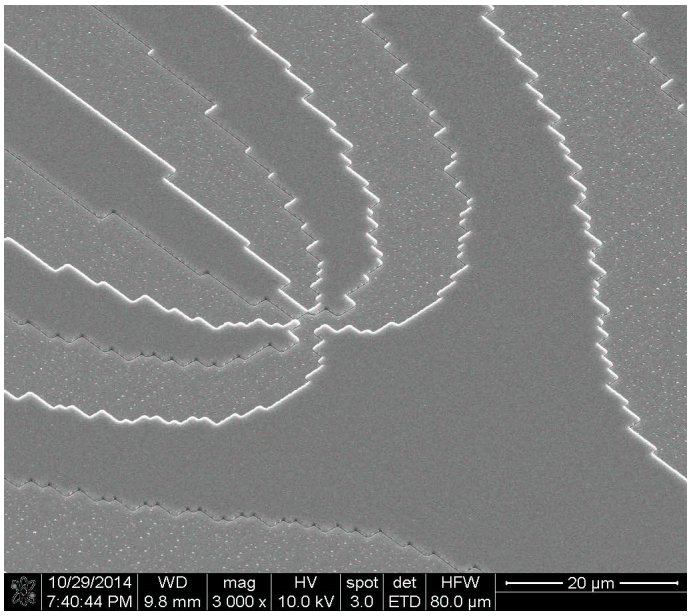

Fig. 14. The SEM image of the fork-like computer hologram which generates optical vortices with $m = 4$ topological charge.

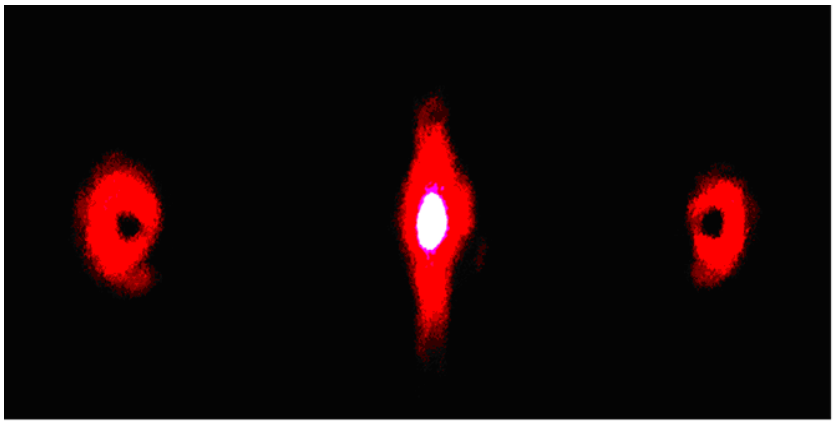

Fig. 15. Far field diffraction image of a Gaussian beam on a reflective fork-like computer generated hologram fabricated with EBL.

5. Conclusions

In this paper we controlled the phase profile of a Gaussian beam and achieved phase singularities called optical vortices with topological charges $m = 2$, $m = 4$ respectively. For this purpose, we applied the beam shaping technique for a 635 nm wavelength radiation using diffractive optical elements. Reflective spiral phase plates and fork-like computer generated hologram, fabricated with reliable nanofabrication techniques such as photolithography and RIE processes for SPPs and electron beam lithography for the fork-like CGH, were used for this purpose. Their high optical quality and diffractive efficiency were proved by structural and functional characterization realized with optical microscope, WLI, SEM or experimental set-up.

Uniform ring intensity was achieved in the optical vortex configurations in radius profile and also zero intensity where the phase was undefined. Phase singularity and Gaussian beam interference was done using a Michelson interferometer in order to determine the topological charge value.

The Matlab simulations based on Kirchhoff's diffraction integral permited the determination of the geometrical parameters necessary for the fabrication of the diffractive optical elements. Their reflective mode configuration facilitated a large flexibility in the experimental set-up manipulation.

Beam shaping simulations results were in concordance with the experimental results.

Acknowledgment. This work has been supported by the project "Secured high volume free space optical communications based on computer generated holograms", UEFISCDI, PN-II-PT-PCCA-2011-3.2-0862 Contract.

References

[1] DICKEY F. M., HOLSWADE S. C., *Laser Beam Shaping: Theory and Techniques*, Marcel Dekker, New York, Basel, 2000.

[2] ROMERO L. A., DICKEY F. M., *Lossless laser beam shaping*, J. Opt. Soc. Am., **A 13**, pp. 751–760, 1996.

[3] HOMBURG O., MITRA T., *Gaussian-to-top-hat beam shaping: an overview of parameters, methods, and applications*, Proc. SPIE **8236**, 82360A, 2012.

[4] ZHANG S., NEIL G., SHINN M., *Single-element laser beam shaper for uniform flat-top profiles*, Opt. Express **11**, pp. 1942–1948, 2003.

[5] MANDEL L., WOLF E., *Optical Coherence and Quantum Optics*, Cambridge University Press,1995.

[6] JACKSON J., *Classical Electrodynamics*, John Wiley & Sons., New York, 1962.

[7] POYNTING J., *The wave motion of a revolving shaft, and a suggestion as to the angular momentum in a beam of circularly polarised light*, Proceedings of the Royal Society of London, **A(82)**, pp. 560–567, 1909.

[8] BETH R. A., *Mechanical Detection and Measurement of the Angular Momentum of Light*, Physical Review, **50**, pp. 115–125, 1936.

[9] ALLEN L., BEIJERSBERGEN M., SPREEUW R., WOERDMAN J., *Orbital angular momentum of light and the transformation of Laguerre-Gaussian laser modes*, Physical Review, **45**(11), pp. 8185–8189, 1992.

[10] CURTIS J. E., GRIER G. D., *Modulated optical vortices*, Optics letters, **28**(11), pp. 872–874, 2003.

[11] KREYSING M. K., KIESS LING T., FRITSCH A., GUCK J. R., JOSEF A. K., *The optical cell rotator*, Optics Express, **16**(21), pp. 912–914, 2008.

[12] LADAVAC K., GRIER D., *Microoptomechanical pumps assembled and driven by holographic optical vortex arrays*, Optics Express, **12**(6), pp. 1144–1149, 2004.

[13] TABOSA J., PETROV D., *Optical Pumping of Orbital Angular Momentum of Light in Cold Cesium Atoms*, Physical Review Letters, **83**(24), pp. 4967–4970, 1999.

[14] ANDREWS D., *Structured Light and Its Applications*, Academic Press, 2008.

[15] HELL S. W., WICHMANN J., *Breaking the diffraction resolution limit by stimulated emission: stimulated-emission-depletion fluorescence microscopy*, Optics Letters, **19**(11), pp. 780–782, 1994.

[16] YAO A. M., PADGETT M. J., *Orbital angular momentum: origins, behavior and applications*, Advances in Optics and Photonics, **3**(2), pp. 161–204, 2011.

[17] GIBSON G., COURTIAL J., PADGETT M., VASNETSOV M., PAS'KO V., BARNETT S., FRANKE-ARNOLD S., *Free-space information transfer using light beams carrying orbital angular momentum*, Optics Express, **12**(22), pp. 5448–5456, 2004.

[18] CAI X., WANG J., STRAIN M. J., JOHNSON-MORRIS B., ZHU J., SOREL M., O'BRIEN J. L., THOMPSON M. G., YU S., *Integrated Compact Optical Vortex Beam Emitters*, Science, **338**(6105), pp. 363–366, 2012.

[19] GROBLACHER S., JENNEWEIN T., VAZIRI A., WEIHS G., ZEILINGER A., *Experimental quantum cryptography with qubits*, New Journal of Physics, **8**(3), pp. 75, 2006.

[20] VASNETSOV M. V., TORRES J. P., PETROV D. V., TORNER L., *Observation of the orbital angular momentum spectrum of a light beam*, Opt. Lett., **28**, pp. 2285–2287, 2003.

[21] KHONINA S. N., KOTLYAR V. V., SHINKARYEV M. V., SOIFER V. A., USPLENIEV G. V., *The phase rotor filter*, Journal of Modern Optics, **39**(3), pp. 1147–1154, 1992.

[22] HE H., HECKENBERG N. R., RUBINSZTEIN-DUNLOP H., *Optical Particle Trapping with Higher-order Doughnut Beams Produced Using High Efficiency Computer Generated Holograms*, Journal of Modern Optics, **42**(1), pp. 217–223, 1995.

[23] TUDOR R., KUSKO M., KUSKO C., CRACIUNOIU F., AVRAM A., VASILACHE D., *Fabrication of spiral phase plates for optical vortices*, Proc. of the CAS–2014 International Conference, **I**, pp. 139–142, 13th–15th October 2014, Sinaia, Romania.

[24] MIYAMOTO Y., MASUDA M., WADA A., TAKEDA M., *Electron-beam lithography fabrication of phase holograms to generate Laguerre-Gaussian beams*, Proc. SPIE **3740**, pp. 232–235, 1999.